Journal of Superconductivity and Novel Magnetism (2020) 33:727–739
https://doi.org/10.1007/s10948-019-05231-4

ORIGINAL PAPER

Physical Properties of Sr-Doped Double Perovskite La_2NiMnO_6

Ting Wang[1] · Hong-Ye Wu[1,2] · Yun-Bin Sun[1,2] · Ru Xing[1,2] · Bao Xv[1,2] · Jian-Jun Zhao[1,2,3]

Received: 22 January 2019 / Accepted: 25 July 2019 / Published online: 8 August 2019

Abstract
A series of double perovskite manganese oxide $La_{2-x}Sr_xNiMnO_6$ ($x = 0, 0.05, 0.1$) samples were prepared by solid-state synthesis. The XRD patterns show that the three samples have perovskite crystal structures. The temperature dependence of the magnetization curves for $La_{2-x}Sr_xNiMnO_6$ ($x = 0, 0.05, 0.1$) near the Curie temperature indicates that Sr-doping weakens the ferromagnetism while enhancing the antiferromagnetism of this system, and the field-dependent magnetization curves further confirm this conclusion. The hysteresis loops, the enlarged views of the hysteresis loops at 2 K, and the Raman spectra of the three samples indicate that Sr-doping increases the antisite disorder degree, the number of antisite defects, and the antiphase boundaries, and the antiferromagnetic coupling between the antiphase boundaries and the surrounding ferromagnetic regions is enhanced. At the same time, the temperature dependence of the inverse magnetic susceptibility changes from an upward deviation from the Curie-Weiss law to a downward trend. This phenomenon can be explained by the opposing changes in the relative strength between the antisite defects and the antiferromagnetic coupling strength. After Sr-doping, the field-cooling curve and field-warming curve of the LSNMO system do not coincide, which is typical of a first-order phase transition. This phenomenon is further confirmed by the rescaling and arrott curves. The temperature dependence of the resistivity curves shows that the $La_{2-x}Sr_xNiMnO_6$ ($x = 0, 0.05, 0.1$) samples are all semiconductor materials. Following Sr-doping, the metal-insulator transition temperature of the system decreases, and the difference between the resistivity values measured at 0 T and 2 T increases.

Keywords Double perovskite · Antisite disorder · Antiphase boundaries · Antiferromagnetic coupling

PACS 75.47.Lx · 91.60.Pn · 75.50.Ee · 75.60.-d

1 Introduction

In recent years, the complex physical properties and wide application value of double perovskite manganese oxides have attracted the attention of domestic and foreign scholars. The general chemical formula of these oxides is $A_2B'B''O_6$. The properties of such compounds are closely related to the arrangement of their B-site ions, and the arrangement of the B-site ions is greatly affected by the synthesis conditions. Therefore, under different preparations and synthesis conditions, the properties of the resultant double perovskite manganese oxides would be very different. The variability in such compounds will affect our understanding of the materials to some extent, but we can regulate the arrangement of the B-site ions by changing the synthesis conditions to control the properties of the materials [1]. J.-S. Kang et al. studied the electronic structure of the double perovskite La_2MnNiO_6 and Sr-doped $La_{1.8}Sr_{0.2}MnNiO_6$ and the valence and spin configuration of the Mn and Ni ions in 2009 [2]. In 2010, Bongjae Kim et al. studied the effects of Sr-doping on the $La_2MnNiO6$ and the antisite disorder in the B-site and found that Sr-doping induced half-metallic properties in $La_{2-x}Sr_xMnNiO_6$, which is related to the antisite disorder at the B-site [3]. Wang et al. used the sol-gel method to prepare La_2NiMnO_6 samples with different particle sizes by changing the synthesis temperature. It was found that the higher the synthesis temperature, the larger the particle size of the sample was, with a larger amount of antisite disorder contained in the particles [4]. Zhou et al. studied the deviation of the temperature

✉ Jian-Jun Zhao
nmzhaojianjun@126.com

[1] Department of Physics, Baotou Normal University, Baotou 014030, China

[2] Inner Mongolia Key Laboratory of Magnetism and Magnetic Materials, Baotou 014030, China

[3] School of Physical Science and Technology, Baotou Teachers College, Baotou, China

dependence of the inverse susceptibility curves from the Curie-Weiss (CW) law for nanosized LNMO and bulk Sr-doped LSNMO samples and discussed the source of the short-range FM order. It was confirmed that the χ^{-1}~T curve of a sample with a large antisite defect will deviate downward from the CW law, and the short-range ferromagnetic (FM) order near the FM transition temperature dominates the system. That is, the short-range FM order originates from the antisite defect [5]. Zhao et al. used the sol-gel method to prepare samples with different particle sizes and determined the effect of the particle size on the physical properties of the samples [6]. Guo et al. prepared the double perovskite manganese oxide $La_{2-x}Sr_xNiMnO_6$ by a solid-phase reaction method and compared the structure, valency, and especially the magnetic properties of a series of samples with different Sr-doping levels. The results showed that Sr-doping leads to an increase in the degree of antisite disorder and an enhancement of the exchange bias (EB) effect [7]. These results have strongly piqued our interest, and we want to refine the doping amount of Sr and study how the antisite defects, magnetic properties, and electrical transport properties of the La_2NiMnO_6 system compared with the undoped sample will be affected if the Sr doping amount is small and the doping amount variation interval is decreased and whether changes in the antisite disorder degree and antiphase boundaries can cause the exchange bias phenomenon. The effects of Sr-doping on the magnetocaloric effect, magnetic phase transition, and electrical properties of the system are also discussed.

2 Experimental Methods

The samples of $La_{2-x}Sr_xNiMnO_6$ ($x = 0$, 0.05, 0.1) were prepared by a conventional solid-phase reaction method. First, high-purity $SrCO_3$, NiO, MnO_2, and La_2O_3 were weighed out according to the stoichiometric ratio, and then anagate ball was added to the mixture, which was ball milled into a powder for 12 h under the protection of petroleum ether [8]. The ground powder was prefired and decarburized at 900 °C for 12 h. Then, the prefired powder was removed, again ball milled with an agate ball and petroleum ether for 12 h, and sintered at 1200 °C for 24 h. The obtained powder sample was thoroughly ground and then sintered at 1350 °C for 24 h. The powder sample was removed, ground again, and calcined at 1450 °C for 24 h to finally obtain smooth, hard, crack-free sheets. The crystal structure of the samples was investigated by X-ray diffraction (XRD), and the electrical properties of the sample were tested by the Physical Property Measurement System (PPMS) manufactured by Quantum Design, Inc., USA. The magnetic properties of the samples were tested using the VSM option of the PPMS.

3 Results and Discussion

Figure 1 shows the results of the refinement of the X-ray diffraction spectra of the $La_{2-x}Sr_xNiMnO_6$ ($x = 0$, 0.05, 0.1) samples by Match! version 3. The undoped sample has a monoclinic structure, and the space group is $P_1\ 2_1/n_1$. After Sr-doping, the sample takes on a tripartite structure, and the space group is $R-3$. As seen from Fig. 1, no significant peaks appear in the diffraction spectra of the samples, so the three samples are in good phase and all form a single phase. After the structure is refined, the lattice parameters of the three samples are obtained, as shown in Table 1. Compared with $La_{1.95}Sr_{0.05}NiMnO_6$, the a-axis and unit cell volume V of the $La_{1.9}Sr_{0.1}NiMnO_6$ sample slightly decrease, and the c-axis slightly increases. The bond length and bond angle of the two samples do not significantly change, which is consistent with the results of Guo etal. [7], indicating that the crystal structure changes among samples with different Sr-doping amounts are not substantial. The tolerance factor t was defined as $t = \frac{(r_A+r_O)}{\sqrt{2}(r_B+r_O)}$, where r_A, r_B, and r_O are the effective radii of the cations at the A and B sites and the oxygen ions, respectively [1]. The ion radii of La^{3+}, Sr^{2+}, Ni^{2+}, Mn^{4+}, and O^{2-} are 0.1032 nm, 0.118 nm, 0.069 nm, 0.053 nm, and 0.14 nm, respectively. According to the calculation, we determined that the tolerance factors of La_2NiMnO_6, $La_{1.95}Sr_{0.05}NiMnO_6$, and $La_{1.9}Sr_{0.1}NiMnO_6$ are 0.8554, 0.8567, and 0.858, respectively, and these values are all between 0.75 and 1.1 and indicate a perovskite crystal structure [8].

The curves in Fig. 2 represent the temperature dependence of the magnetization for the samples with Sr-doping amounts of $x = 0$, $x = 0.05$, and $x = 0.1$ in a magnetic field of 5 mT. The Curie temperature T_C of the three samples is approximately 280 K, indicating that an FM transition occurs around room temperature in the samples. J.-S. Kang et al. performed the 2p X-ray absorption spectroscopy (XAS) of Mn and Ni of $La_{2-x}Sr_xMnNiO_6$ ($x = 0$, 0.2) in 2009. Comparing the Mn 2p XAS spectra with the reference Mn 2p XAS spectra of the Mn oxides MnO_2 (Mn^{4+}), Mn_2O_3 (Mn^{3+}), and MnO (Mn^{2+}), it is found that the Mn 2p XAS spectra of $x = 0$ and $x = 0.2$ are close to each other, distinctly different from Mn_2O_3 (Mn^{3+}) and MnO (Mn^{2+}) but similar to MnO_2 (Mn^{4+}), which can be well described by the calculated Mn^{4+} XAS; that is, the Mn ion in $La_{2-x}Sr_xMnNiO_6$ ($x = 0$, 0.2) is tetravalent. The Ni 2p XAS spectra of the Ni ions are compared with the Ni (Ni^{2+}) and Pr NiO_3 (Ni^{3+}) Ni 2p XAS spectra. The Ni 2p XAS spectra of NiO (Ni^{2+}) are well fitted to the calculated Ni 2p XAS spectra of Ni^{2+}, indicating that the Ni ions in $La_{2-x}Sr_xMnNiO_6$ ($x = 0$, 0.2) are divalent [2]. Therefore, the T_C of our samples is close to room temperature, probably because this ferromagnetic transition is due mainly to the superexchange interaction between Ni^{2+} and Mn^{4+} [5]. The T_C of LNMO depends on the FM coupling strength between the Ni and Mn ions, while the bond

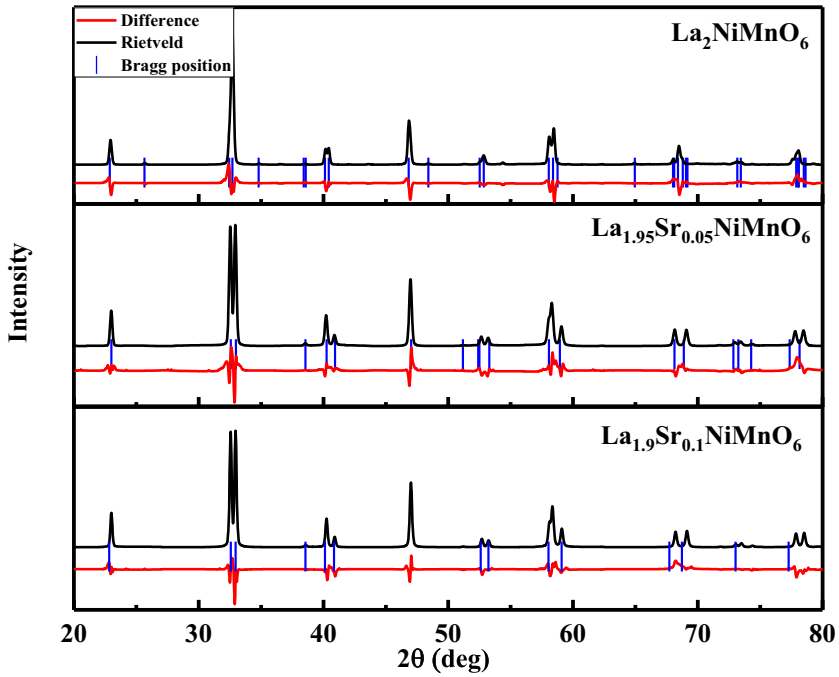

Fig. 1 XRD patterns of the $La_{2-x}Sr_xNiMnO_6$ ($x = 0$, 0.05, 0.1) samples

length and bond angle of Ni^{2+}-O^{2-}-Mn^{4+} and the structural parameters may affect the FM coupling strength [7, 9]. Figure 2 shows that the Curie temperature of the three samples changes only slightly with Sr-doping, indicating that the FM coupling strength in the system is not significantly affected by Sr-doping. The field-cooled (FC) curves of the three samples show similar trends, and the intensity of the magnetization increases with the decreasing temperature. The magnetization of the undoped sample La_2NiMnO_6 is 0.12 $\mu_B/f.u.$ near 10 K, and when the doping amount of Sr is $x = 0.05$ and $x = 0.1$, the magnetization decreases to 0.08 $\mu_B/f.u.$ and 0.027 $\mu_B/f.u.$, respectively, near 10 K. Sr-doping also results in the overall magnetization of the zero-field cooled (ZFC) curves of the three samples decreasing, which indicates that Sr-doping weakens the ferromagnetism and enhances the antiferromagnetism of the system [10]. For the three samples, the FC and ZFC curves clearly bifurcate below T_C, and a transition point exists on the ZFC curve due to the interaction between the FM and AFM components. This interaction is very common in heterogeneous FM materials, spin glass, and cluster glass systems [11].

Figure 3 shows isothermal M-H curves for the $La_{2-x}Sr_xNiMnO_6$ ($x = 0$, 0.05, 0.1) samples near the Curie temperature. The results indicate that Sr-doping significantly reduces the spontaneous magnetization of different samples at the same temperature; the slopes of the curves decrease at the low-field region and increase at the high-field region, indicating that the ferromagnetism is weakened in the system while the antiferromagnetism is enhanced [12], which is consistent with the conclusion from Fig. 2. Moreover, when the Sr-doping amount reaches $x = 0.1$, the M-H curves of the sample in the high-field region are almost linear, indicating that the AFM phase dominates in the sample compared with the sample with a lower Sr-doping amount and the undoped sample. A large number of AFM antisite disorders, Ni^{2+}-O-Ni^{2+} and Mn^{4+}-O-Mn^{4+}, are present in the $La_{1.9}Sr_{0.1}NiMnO_6$ system [13].

Table 1 Lattice parameters of the $La_{2-x}Sr_xNiMnO_6$ ($x = 0$, 0.05, 0.1) samples

x	a (A°)	b (A°)	c (A°)	v ($A^{3\circ}$)
0	5.5079	5.4575	7.7332	232.45
0.05	5.4983	–	13.2296	346.35
0.1	5.4965	–	13.2313	346.18

The general chemical formula of a double perovskite is $A_2BB'O_6$. In a perfectly ordered double perovskite structure, B and B′ will occupy unique crystallographic positions, e.g., 2c (1/2, 0, 0) and 2d (0, 1/2, 0), and be alternatingly arranged along the entire crystal, i.e., each B coordinates with only a specific B′, and vice versa. However, the occupancy of 2c and 2d is uncertain, and B and B′ can both occupy these two positions, which leads to the random arrangement of B and B′ in our actual synthesis process and the formation of the well-known "antisite disorder" [13, 14]. The synthesis and annealing conditions determine the antisite disorder degree of samples to a large extent [13, 15]. The number of antisite disorders increases when a threshold is reached, APBs form, and APBs are antiferromagnetically coupled with the surrounding FM region [4]. We cooled samples to 10 K from 300 K with an applied magnetic field of 10 T. Figure 4 shows the magnetic field dependence of the magnetization in the range of − 80–80 kOe. After doping with Sr, the saturation

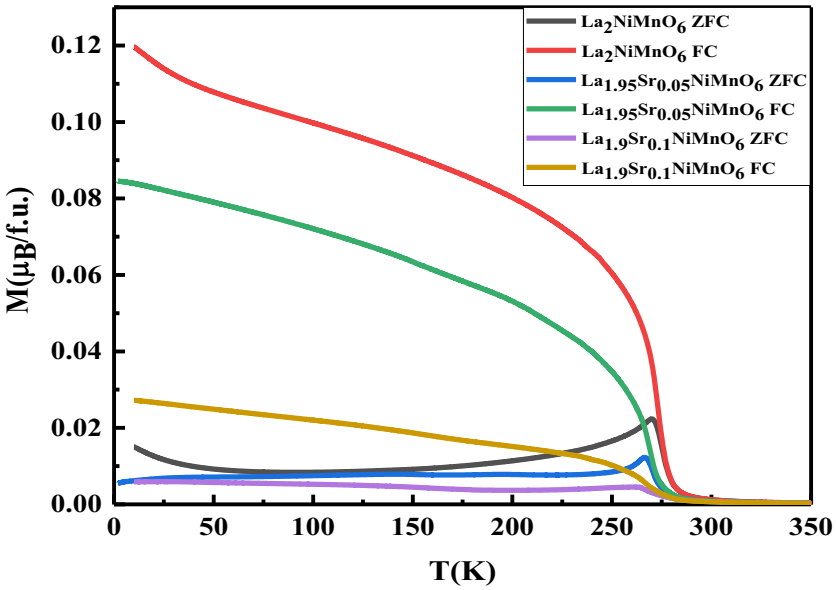

Fig. 2 Temperature dependence of magnetization for $La_{2-x}Sr_xNiMnO_6$ ($x = 0$, 0.05, 0.1) in a magnetic field of 5 mT

magnetization of the samples decreases; with a magnetic field of 8 T, if all Ni^{2+} and Mn^{4+} ions are in a completely FM arrangement, the theoretical value of the saturation magnetization is 5 $\mu_B/f.\ u.$ [10, 12, 13]. The saturation magnetization of the double perovskite $La_{2-x}Sr_xNiMnO_6$ ($x = 0$, 0.05, 0.1) samples is 2.62 $\mu_B/f.\ u.$, 2.3 $\mu_B/f.\ u.$ and 2.05 $\mu_B/f.\ u.$, respectively, which are obviously smaller than the theoretical value. This shows that antisite disorders exist in the undoped LNMO system, and with the doping of Sr, the antisite disorder degree of the LSNMO system increases [7, 16–18]. To further illustrate this phenomenon, we plotted the ratio of the magnetization intensity to the saturation magnetization as a function

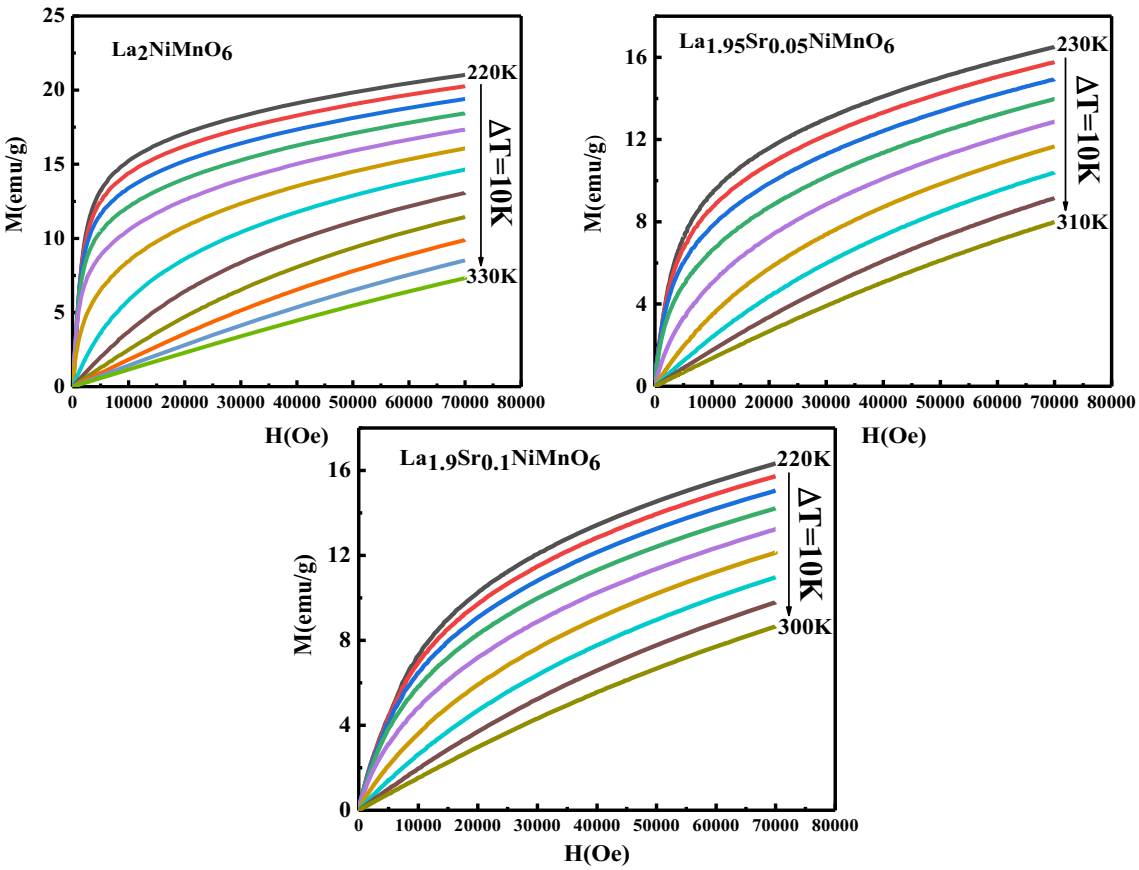

Fig. 3 Field-dependent magnetization of $La_{2-x}Sr_xNiMnO_6$ ($x = 0$, 0.05, 0.1) near the Curie temperature

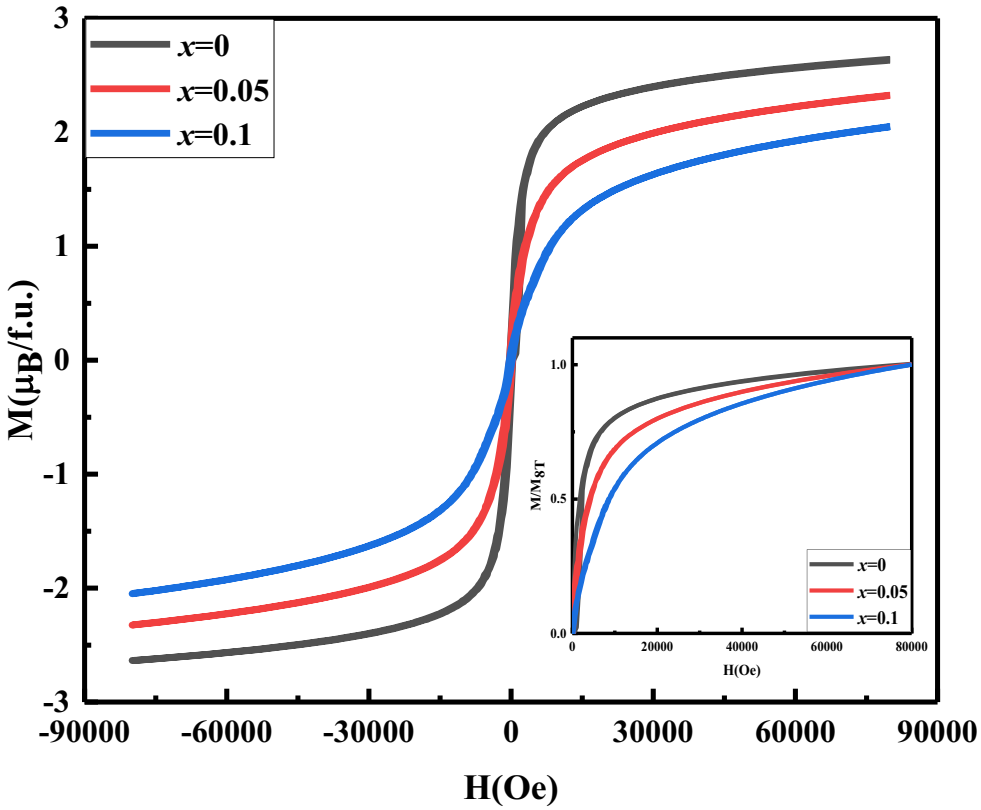

Fig. 4 Hysteresis loops for $La_{2-x}Sr_xNiMnO_6$ ($x = 0$, 0.05, 0.1) samples at 10 K

of the magnetic field, as shown in the inset of Fig. 4. The slopes of the curves increase at a high magnetic field as the Sr-doping amount increases; in other words, the difference between the magnetization at a high magnetic field and the maximum magnetization value that each sample can achieve at 8 T is increased. In fact, the sample with a Sr-doping amount of $x = 0.1$ does not completely reach saturation at 8 T. This result indicates that when the Sr-doping amount is larger, the magnetization saturation of the system is harder to achieve, and thus, a larger saturation magnetic field is required. The reason for this phenomenon is that Sr-doping in the LNMO system causes the formation of APBs in the system, and AFM coupling occurs between the APBs and the surrounding FM regions. As the Sr-doping amount increases, the antiferromagnetic coupling is enhanced [4].

Bongjae Kim et al. reported in 2010 that the X-ray magnetic circular dichroism (XMCD) signal of $La_{1.8}Sr_{0.2}MnNiO_6$ is weaker than that of La_2MnNiO_6, which is attributed to the antisite disorder of the B-site Mn/Ni ions, which will affect the structure and magnetic properties of the system. These researchers used band structure calculations to test the effect of the antisite disorder on the electrical and magnetic properties of the $La_{2-x}Sr_xMnNiO_6$ system for the incompletely ordered system of B-site Mn/Ni [3]. Within the experimental methods, it is widely accepted that Raman spectra are used to describe the antisite disorder degree of double perovskite oxides [6, 19, 20]. In a previous work, Guo et al. studied the Raman spectra of completely ordered LNMO samples and LNMO films with disordered Ni/Mn and found that the bands of both samples that appeared at approximately 540 cm^{-1} and 680 cm^{-1} represent the antistretching (AS) and stretching (S) vibrations of $(Ni/Mn)O_6$ octahedra. The peak intensity in the Raman spectra of the disordered Ni/Mn film was weaker at both positions, and the peak width was broader [19]. Therefore, we obtained the Raman spectra of the three samples at room temperature to verify the change in the antisite disorder degree of the samples with Sr-doping. As shown in Fig. 5, two peaks appear in the vicinity of 540 cm^{-1} and 680 cm^{-1}, corresponding to the AS and S modes, respectively. As the Sr-doping amount increases, the spectral intensity of the peaks at these two sites gradually decreases; the inset of Fig. 5 shows the full width at half maximum (FWHM) values of the AS and S peaks. The FWHM monotonically increases with the increasing Sr doping amount at 540 cm^{-1}, while the FWHM of the peak at approximately 680 cm^{-1} for $La_{1.95}Sr_{0.05}NiMnO_6$ is slightly lower than that of La_2NiMnO_6. The FWHM of $La_{1.9}Sr_{0.1}NiMnO_6$ is significantly greater than that of $La_{1.95}Sr_{0.05}NiMnO_6$ and La_2NiMnO_6, showing a nonmonotonic change. These changes indicate that when the Sr-doping amount is small, the antisite disorder degree in the sample with Sr-doping is not much different from that of an undoped sample; when the Sr doping amount reaches $x = 0.1$, a larger antisite disorder degree is observed.

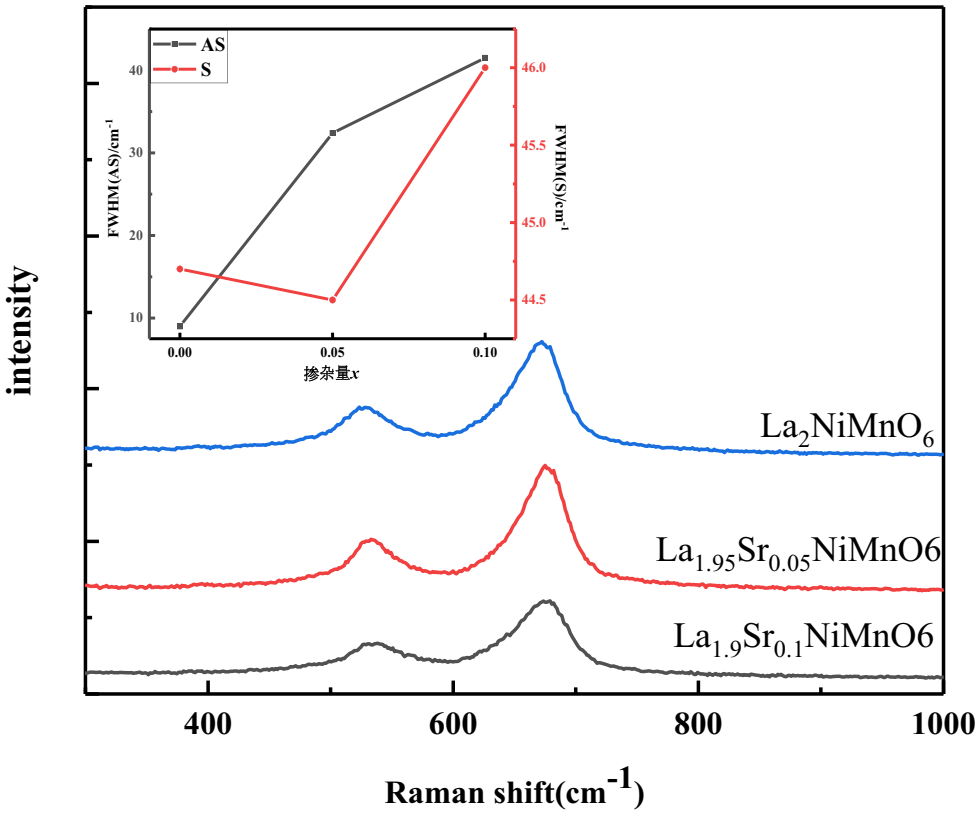

Fig. 5 Raman spectra at room temperature for $La_{2-x}Sr_xNiMnO_6$ ($x = 0, 0.05, 0.1$)

In Sect. 1, we briefly described the work of Zhou et al. and Wang et al.; these works are discussed in detail here. Zhou et al. [5] studied the deviation of the temperature dependence of the inverse magnetic curves from Curie's law (the CW law) of bulk LNMO, bulk LSNMO, and nanoscale LNMO samples in the vicinity of the FM transition temperature. Among the samples, the bulk LNMO sample had the smallest antisite defect, and its χ^{-1}~T curve deviated upward from the CW law. The antisite defect of the bulk LSNMO sample was larger, and its χ^{-1}~T curve still deviated upward from the CW law near the FM transition temperature. However, the nanoscale LNMO sample has the largest antisite defect, and its χ^{-1}~T curve deviated downward from the CW law near the FM transition temperature; at this point, the short-range FM order is dominant near the FM transition temperature, and the conclusion is that the short-range FM order originates from the antisite defect. Wang et al. [4] controlled the particle size by changing the synthesis temperature and studied the relationship between the particle size and magnetic properties, especially the effects of the AFM coupling strength on the magnetic properties. Their results showed that if the antisite disorder degree in the system is large, then an AFM interaction will exist among the antisite disorders and tend to form an APB; however, if the particle size of the sample is small, the antisite disorders tend to distribute independently, and the AFM coupling is weakened. The above two conclusions show that the short-range FM order tends to cause the χ^{-1}~T curve to deviate downward from the CW law, while the AFM coupling among the antisite disorders tends to cause the curve to deviate upward from the CW law, which are two opposite deviation trends. Thus, whether the χ^{-1}~T curve deviates upward or downward from the CW law near the FM transition temperature depends on whether the system is dominated by the short-range FM order or AFM coupling.

We show the temperature dependence of the inverse magnetic susceptibility curves of the three samples measured with an applied magnetic field of 50 Oe in Fig. 6. Compared with $La_{1.95}Sr_{0.05}NiMnO_6$ and $La_{1.9}Sr_{0.1}NiMnO_6$, the undoped sample La_2NiMnO_6 has fewer antisite defects and the weakest AFM coupling strength among the antisite disorders, and the temperature dependence of its inverse magnetic susceptibility curve χ^{-1}~T begins to deviate upward from the CW law above the Griffith temperature of $T_G \approx 320$K. A short-range AFM order begins to appear in the system, indicating that the AFM coupling has a greater influence on the La_2NiMnO_6 system than the antisite defects. In the $La_{1.95}Sr_{0.05}NiMnO_6$ sample, the antisite defects increase, the AFM coupling increases, and the χ^{-1}~T curve starts to deviate from the CW law in the vicinity of $T_G \approx 305K$. The system begins to have short-range AFM order, indicating that the influence of the AFM interaction in the $La_{1.95}Sr_{0.05}NiMnO_6$ system is still greater than that of the short-range FM order, but the χ^{-1}~T curve deviation from the CW law is less than that observed for the undoped sample. With $La_{1.9}Sr_{0.1}NiMnO_6$, the antisite

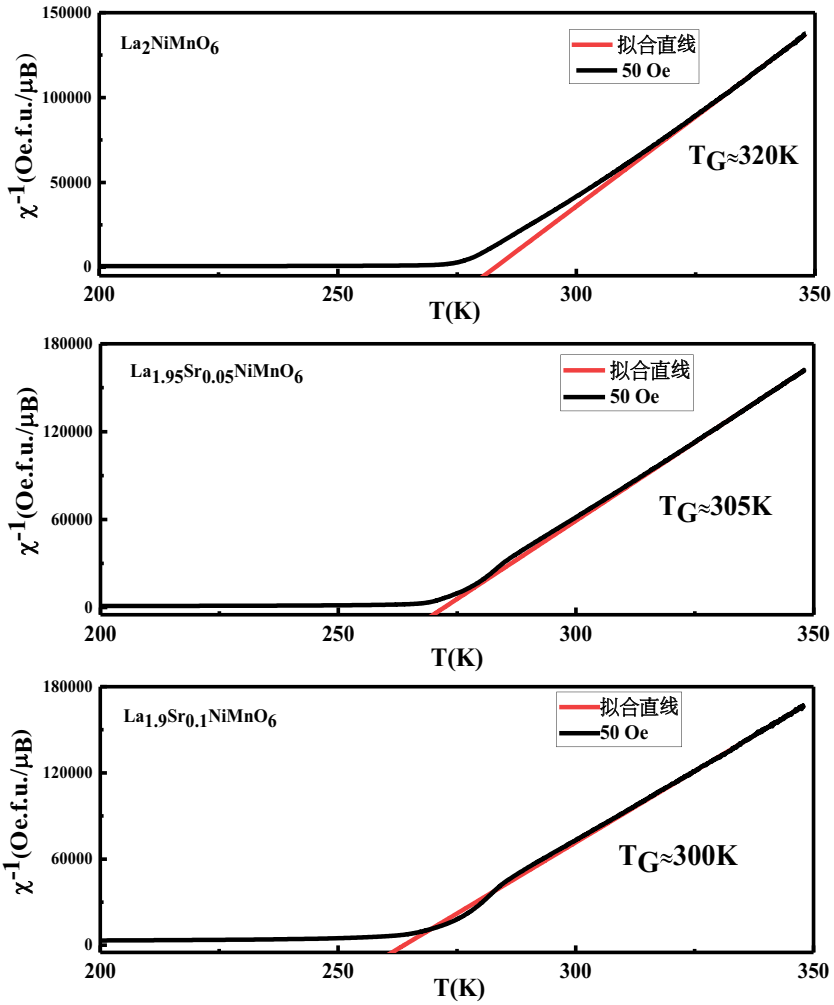

Fig. 6 Temperature-dependent χ^{-1} under 5 mT for $La_{2-x}Sr_xNiMnO_6$ ($x = 0, 0.05, 0.1$)

defects in the system reach a maximum, and the AFM coupling strength is the strongest relative to that of the other samples. The χ^{-1}~T curve starts to deviate downwards from the CW law in the vicinity of $T_G \approx 300K$. This result shows that the influence of the short-range FM order on the system is greater than that of the AFM coupling; the short-range FM order is dominant near the FM transition temperature, which destroys the long-range FM order of the system [21].

The research of Nyrissa et al. revealed that if the space conditions are suitable, the antisite disorder degree of a system is very high, and once the coupling strength increases to a certain threshold, APBs tend to form [22]. For LNMO, based on the superexchange rule, AFM coupling occurs between Ni^{2+}-O^{2-}-Ni^{2+} and Mn^{4+}-O^{2-}-Mn^{4+}, forming AFM APBs and leading to the coexistence of FM domains and antisite boundary APBs in the system. A large magnetic field can be applied to cool the sample from a temperature above the Neel temperature, and then APBs antiferromagnetically couple with the ferromagnetic domain at the interface, which may lead to an exchange bias phenomenon [1, 22, 23]. The value of the exchange bias field H_E is $|H_E| = |-(H_1+H_2)/2|$, and the value of the coercive field H_C is $|H_C| = |(H_2-H_1)/2|$. We cooled three samples from 300 to 2 K with an applied magnetic field of 1 T and examined the hysteresis loops at 10 K. Figure 7 a–c shows the enlarged views in the low magnetic field region for La_2NiMnO_6, $La_{1.95}Sr_{0.05}NiMnO_6$, and $La_{1.9}Sr_{0.1}NiMnO_6$, and Fig. 7d shows the exchange bias fields and coercive fields of the three samples. The coercive fields of the three samples are 404.5 Oe, 398.5 Oe, and 355 Oe, respectively, and the field monotonically decreases with the increasing Sr-doping amount. This decrease is because as the Sr-doping amount increases, although the AFM spin increases, the FM component is also obviously weakened, leading to the anisotropy of the FM component decreasing and causing the coercive field of the sample to gradually decrease with the increase in the Sr-doping amount [7]. The exchange bias fields of La_2NiMnO_6, $La_{1.95}Sr_{0.05}NiMnO_6$, and $La_{1.9}Sr_{0.1}NiMnO_6$ are very small, 5.5 Oe, 15.5 Oe, and 55 Oe, respectively, but it can be seen that the exchange bias increases monotonically with the doping of Sr. In the classical Meiklejohn and Bean relationship [23], the exchange bias field is defined as $H_E = JS_{AFM}S_{FM}/\mu_0 t_{FM}M_{FM}$, where J is the exchange constant of the unit area along the

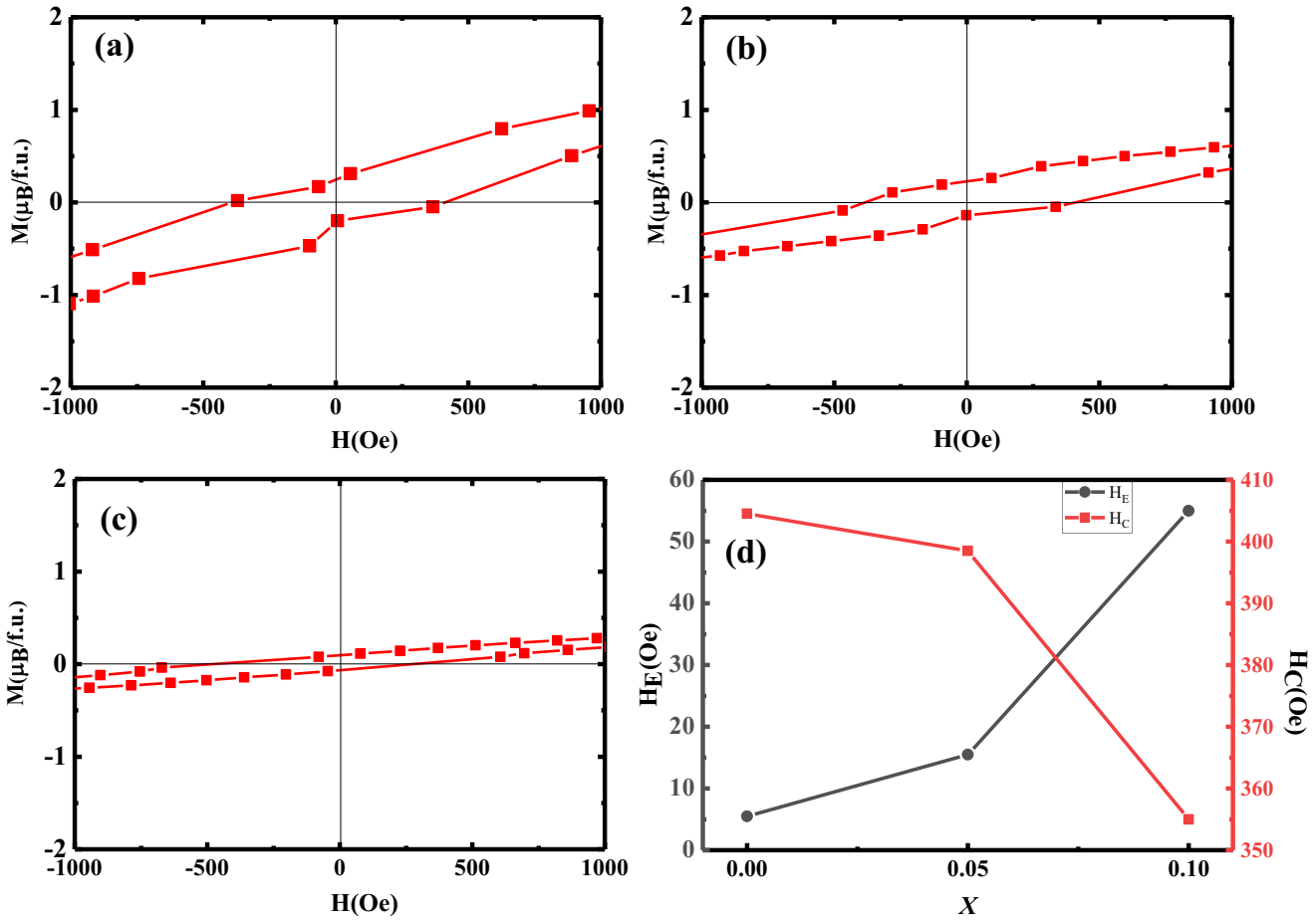

Fig. 7 **a**–**c** Enlarged views of the low-field hysteresis loops at 2 K under the FC process with a cooling field of 1 T for $La_{2-x}Sr_xNiMnO_6$ ($x = 0, 0.05, 0.1$). **d** H_E field and coercive field for $La_{2-x}Sr_xNiMnO_6$ ($x = 0, 0.05, 0.1$)

FM/AFM interface, S_{AFM} and S_{FM} are the interfacial AFM and FM magnetizations, respectively, and the product of $t_{FM}M_{FM}$ in the denominator represents the total magnetization of the FM component. With an increase in the Sr-doping amount, the antisite disorder degree, the intensity of the AFM spin at the interface, and the interface magnetization all increase. Figure 4 shows that doping with Sr causes the saturation magnetic field of the system to increase and the coupling between the APBs and the FM component to increase. Although the exchange bias phenomenon is not obvious in our three samples, from the phenomenon that as the Sr-doping amount increases the exchange bias field of the system monotonically increases combined with Figs. 2, 3, and 4, it is well confirmed that Sr-doping does cause an antiferromagnetism enhancement of the system. When the ferromagnetism is weakened, the total magnetization of the FM component is reduced.

In previous research, few scholars have discussed the magnetocaloric effect of the $La_{2-x}Sr_xNiMnO_6$ series. Thus, based on the classical theory of thermodynamics, we obtained the magnetic entropy change value by calculating the M-H data of the samples:

$$|\Delta S| = \int_0^{H_{max}} \left(\frac{\partial S}{\partial H}\right)_T dH \tag{1}$$

According to Maxwell's equation:

$$\left(\frac{\partial M}{\partial T}\right)_H = \left(\frac{\partial S}{\partial H}\right)_T \tag{2}$$

We obtained:

$$|\Delta S| = \int_0^{H_{max}} \left(\frac{\partial M}{\partial T}\right)_H dH \tag{3}$$

Using a numerical approximation for Eq. (3), we can obtain the following:

$$|\Delta S| = -\sum_i \frac{M_{i+1} - M_i}{T_{i+1} - T_i} \Delta H_i \tag{4}$$

where M_{i+1} and M_i in the expression are the magnetization values corresponding to the temperatures T_{i+1} and T_i, respectively, and H_i is the applied magnetic field [24]. The magnetic

entropy change value can be obtained by substituting the corresponding value into Eq. (4). Figure 8 shows the temperature dependence of the magnetic entropy for the $La_{2-x}Sr_xNiMnO_6$ ($x = 0$, 0.05, 0.1) samples, and the maximum values of the magnetic entropy under a magnetic field of 7 T are $-1.38\ J \cdot kg^{-1} \cdot K^{-1}$, $-0.98\ J \cdot kg^{-1} \cdot K^{-1}$, and $-0.83\ J \cdot kg^{-1} \cdot K^{-1}$, respectively.

The maximum magnetic entropy values of the three samples in different magnetic fields appear in the vicinity of the Curie temperature T_C. The temperature corresponding to the maximum magnetic entropy of the undoped sample under different magnetic fields is basically the same, but when Sr is $x = 0.05$ and $x = 0.1$, the temperature corresponding to the maximum magnetic entropy changes slightly with the change in the magnetic field, indicating that a magnetic phase transition may occur in the system [25].

Figure 9 shows the field-cooling curves (FCCs) and field-warming curves (FCWs) of La_2NiMnO_6, $La_{1.95}Sr_{0.05}NiMnO_6$ and $La_{1.9}Sr_{0.1}NiMnO_6$ in the range of 250–300 K. It can be seen that thermal hysteresis exists in the three samples near the Curie temperature, i.e., there is an obvious mismatch between the FCCs and FCWs, which is a typical feature of a first-order phase transition in the system [26]. According to the rescaling curves and the arrott curves, it can be further determined whether there is a first-order phase transition in the sample. The *y*-axis is the ratio of each magnetic entropy value to the maximum magnetic entropy value under the studied magnetic field, and the abscissa of the rescaling curves is

$$\theta = \begin{cases} -(T-T_C)/(T_1-T_C) & T \le T_C \\ (T-T_C)/(T_2-T_C) & T \ge T_C \end{cases}$$

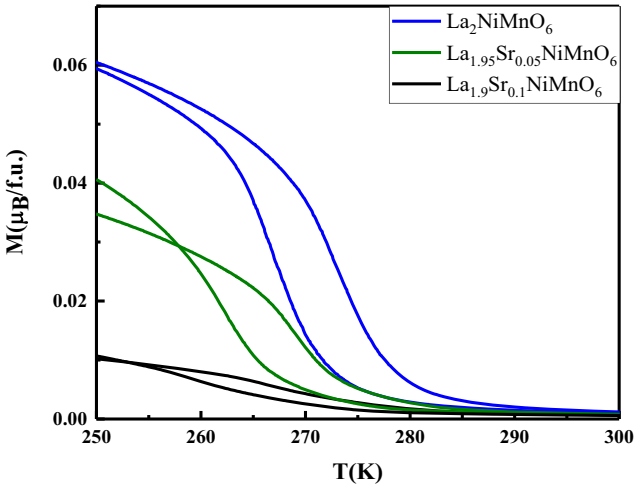

Fig. 9 Temperature-dependent magnetization curves for $La_{2-x}Sr_xNiMnO_6$ ($x = 0$, 0.05, 0.1) samples upon warming and cooling in a magnetic field of 5 mT

T_1 and T_2 in the formula can be calculated by $\Delta S(T_1)/\Delta S_M^P = \Delta S(T_2)/\Delta S_M^P = 0.5$ [24]. Franco et al. noted that if the rescaling curve for each magnetic field can fall on the same main curve, the material has undergone a second-order phase transition; if the rescaling curve for each magnetic field does not fall on the same main curve but shows a diffuse distribution, the material has undergone a first-order phase transition [25]. Wang DH et al. noted that if the arrott curves in the vicinity of a certain temperature have a negative slope or an S-shape, there is a first-order phase transition near that temperature; if the slope of the curves is positive or if the curves are parallel to each other, the system has undergone a second-order phase transition [27, 28].

Using the temperature dependence data from the magnetic entropy and isothermal magnetization curves (M-H), the rescaling and arrott curves of the $La_{2-x}Sr_xNiMnO_6$ ($x = 0$, 0.05, 0.1) samples were created and are shown in Fig. 10 a, c, e and Fig. 10 b, d, f. For the undoped sample, La_2NiMnO_6,

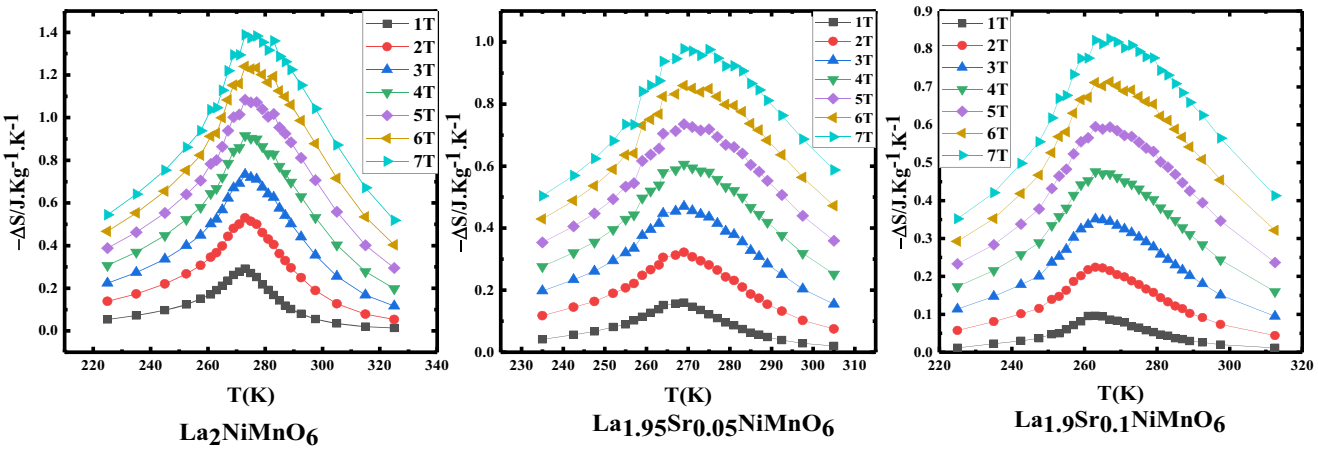

Fig. 8 $\Delta S - T$ curves of $La_{2-x}Sr_xNiMnO_6$ ($x = 0$, 0.05, 0.1)

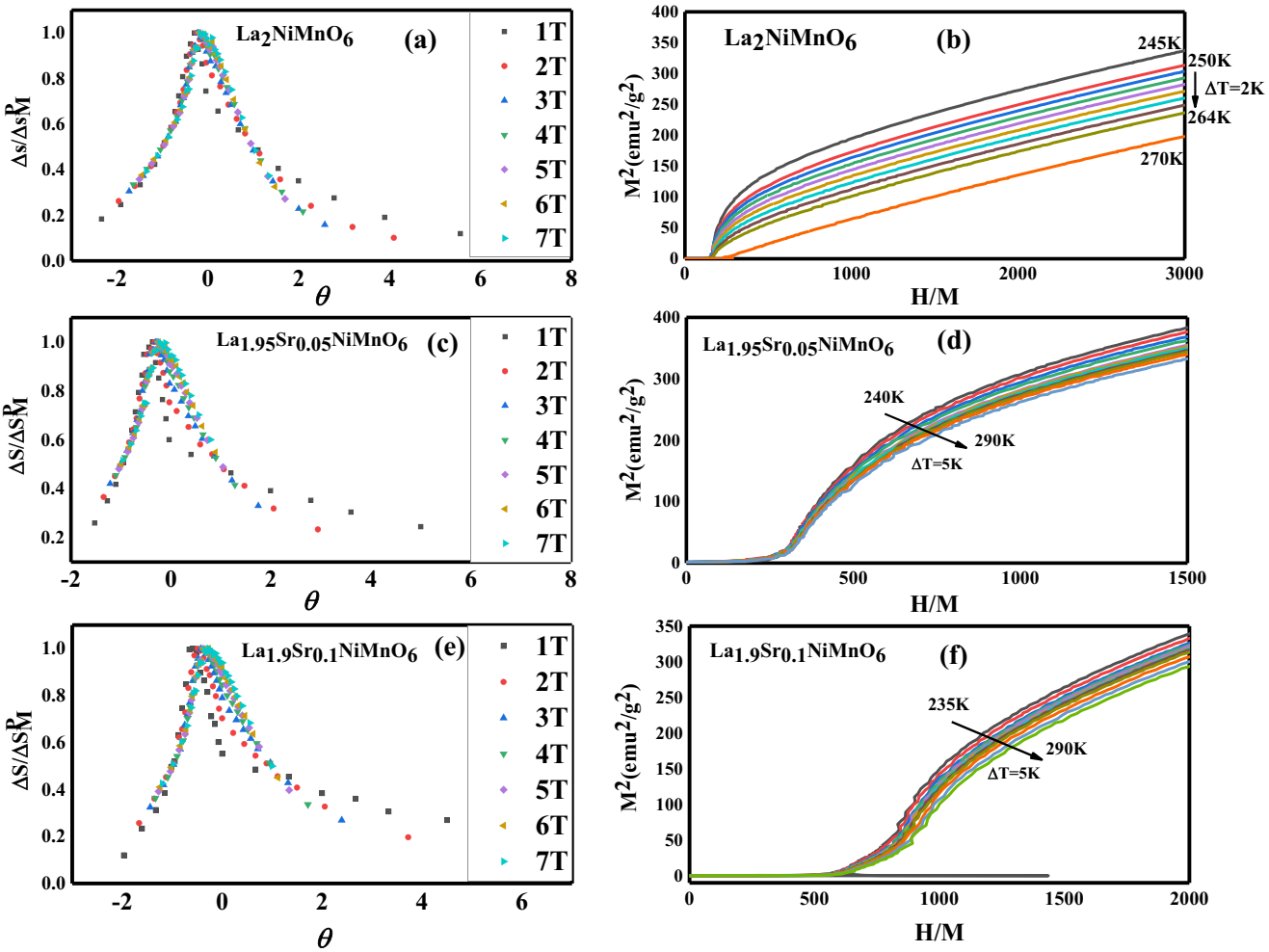

Fig. 10 Panels (**a**), (**c**), and (**e**) are rescaling curves for $La_{2-x}Sr_xNiMnO_6$ ($x = 0, 0.05, 0.1$) samples and panels (**b**), (**d**), and (**f**) are $M^2 - H$ curves for $La_{2-x}Sr_xNiMnO_6$ ($x = 0, 0.05, 0.1$) samples

the curve shows a slightly diffuse distribution, but the arrott curve does not show a significant negative slope, and the curves are substantially parallel. Some of the selected curves are shown in Fig. 10b. For the sample with a Sr-doping amount of $x = 0.05$, the rescaling curves for each magnetic field do not fall on the same main curve, and the curves exhibit a diffuse distribution. We used the isothermal magnetization curves to obtain the arrott curves in the temperature range of 240–290 K. The shape of the curves was observed to be S-shaped, indicating that the $La_{1.95}Sr_{0.05}NiMnO_6$ system experiences a weak first-order phase transition, causing the misalignment between the FCCs and FCWs. For the sample with a Sr-doping amount of $x = 0.1$, the rescaling curves for each magnetic field do not fall on the same main curve, and the curves also exhibit a diffuse distribution. We obtained the arrott curves in the temperature range of 235–290 K, and the curves generally show a distinct S-shape. The FCCs and FCWs also do not coincide at 60 K for the $La_{1.9}Sr_{0.1}NiMnO_6$ sample due to the weak first-order phase transition in the system.

To study the effect of Sr-doping on the electrical properties of the $La_{2-x}Sr_xNiMnO_6$ samples, we tested the temperature dependence of the resistivity of the three samples at 0 T, as shown in Fig. 11. The resistivities of the three samples are all in the range of 0–7000 $\Omega \cdot m^{-3}$, and the values are between 10^{-3} and 10^9. The experimental data for the three samples were fitted with $\ln(\rho) - T^{-1/4}$ curves, and the fitting results show that all three samples follow the variable range hopping conductivity model, as shown in the illustration [29], indicating that the conductivities of the systems do not change substantially with Sr-doping and that the three samples are all semiconductor materials. Bongjae Kim et al. studied the effects of antisite disorders on the magnetic and electrical properties of Lb_2MnNiO_6. In Lb_2MnNiO_6 with ordered/antisite disorder Mn/Ni and an assumed FM/AF spin configuration for the disordered system, the total densities of states (DOS) for Lb_2MnNiO_6 with antisite disorder at the B sites in the virtual atom method, except for the different atomic orderings and spin configurations, in the three cases of ordered FM (OFM), disordered AF (DAF) and disordered FM (DFM),

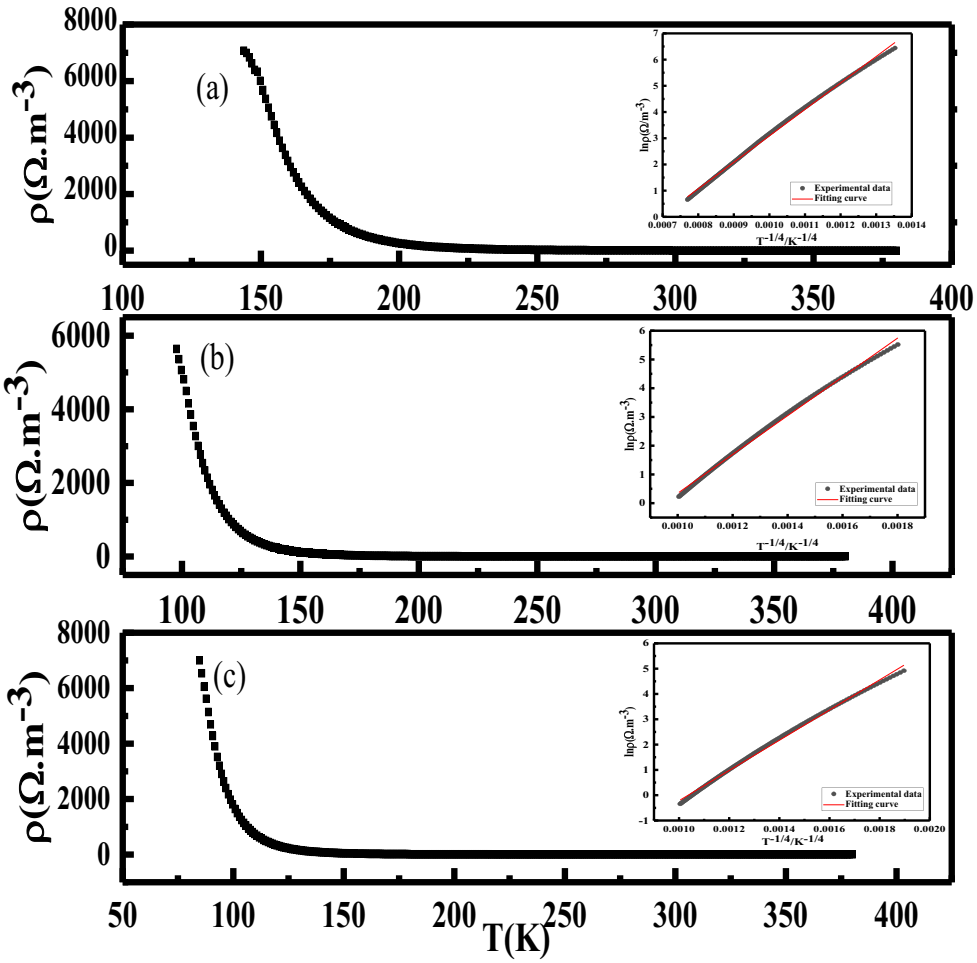

Fig. 11 **a** Temperature dependence of the resistivity of La_2NiMnO_6 in a magnetic field of 0 T. **b** Temperature dependence of the resistivity of $La_{1.95}Sr_{0.05}NiMnO_6$ in a magnetic field of 0 T. **c** Temperature dependence of the resistivity of $La_{1.95}Sr_{0.05}NiMnO_6$ in a magnetic field of 0 T. The insets show the ln $(\rho) - T^{-1/4}$ curves for $La_{2-x}Sr_xNiMnO_6$ (x = 0, 0.05, 0.1)

are similar to each other, indicating that when the B-site disorder degree is small, it does not have much influence on the system's electrical properties, although the magnetic exchange interaction between a small part of the transition metal (TM) element has changed [3]. This conclusion theoretically confirms our experimental results. Sr-doping caused and increased the antisite disorder in our $La_{2-x}Sr_xNiMnO_6$ ($x = 0$, 0.05, 0.1) system, but the antisite disorder was not great enough to change the electrical properties of the system. However, as shown in Fig. 11, the metal-insulator transition temperatures of La_2NiMnO_6, $La_{1.95}Sr_{0.05}NiMnO_6$, and $La_{1.9}Sr_{0.1}NiMnO_6$ are approximately 175 K, 140 K, and

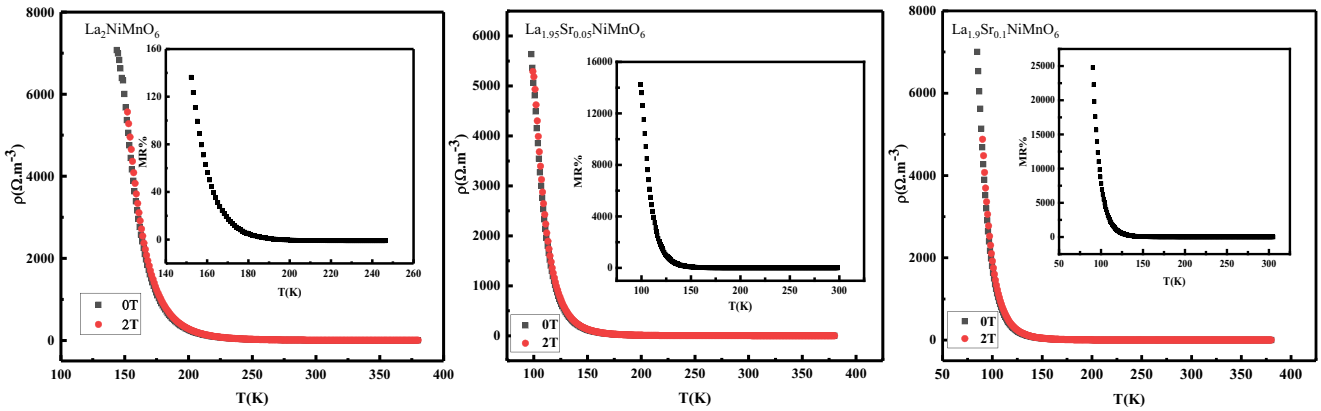

Fig. 12 Temperature dependence of resistivity of $La_{2-x}Sr_xNiMnO_6$ ($x = 0$, 0.05, 0.1) in magnetic fields of 0 T and 2 T. The inset shows the magnetoresistance of $La_{2-x}Sr_xNiMnO_6$ ($x = 0$, 0.05, 0.1)

125 K, respectively, which shows that the metal-insulator transition temperature of the system monotonically decreases with the increasing Sr-doping amount.

In Fig. 12, we compared the temperature dependence of the resistivity under applied fields of 0 T and 2 T for the three samples and found that the magnetic field had no effect on the transition temperature. The transition temperature does not shift after applying a magnetic field, but the maximum resistivity that can be achieved for the three samples decreases, indicating that the magnetic field has an inhibitory effect on the resistivity. Figure 12 shows the temperature dependence of MR% for the three samples, $MR(T)\% = [\rho(T)_{2T} - \rho(T)_{0T}]/\rho(T)_{0T}$, which can be used to determine the degree of influence that the magnetic field has on the different samples. It can be seen from the illustrations that the MR% increases with the doping of Sr, indicating that the difference between the resistivity with a magnetic field of 0 T and the resistivity with a magnetic field of 2 T increases. Thus, the influence of the magnetic field on the resistivity has become more obvious [7].

4 Conclusion

Well-formed samples of $La_{2-x}Sr_xNiMnO_6$ ($x = 0$, 0.05, 0.1) were prepared by a solid-phase reaction. The Sr doping of the system weakens the ferromagnetism, enhances the AFM properties, decreases the saturation magnetization, and increases the saturation magnetic field. The intensity of the bands in the Raman spectra decreases, and the width of the bands increases. The exchange bias phenomenon becomes more obvious, the exchange bias field monotonically increases, and the coercive field monotonically decreases. The curve of the temperature dependence of the inverse magnetic susceptibility (χ^{-1}~T) changes from an upward deviation from the CW law near the FM transition temperature to a downward deviation from the CW law near the FM transition temperature. These results show that as the Sr-doping amount increases, the antisite disorder degree of the system increases, and the number of antisite defects increases. As a result, the intensity of the AFM coupling between APBs and the adjacent FM regions increases. In addition, Sr-doping leads to a short-range FM order enhancement, and the magnetic behavior of the system is determined by the short-range FM order. The long-range FM order of the system is suppressed. At the same time, doping with Sr causes the system to undergo a weak first-order phase transition, but Sr-doping has little effect on the conductivity of the LNMO system. All three samples exhibit semiconductor characteristics, but with the Sr-doping, the metal-insulator transition temperature of the samples decreases, and the influence of the magnetic field on the resistivity increases. Meanwhile, the magnetoresistance effect becomes more obvious.

Funding Information Project supported by the National Natural Science Foundation of China (Grant Nos. 11164019, 51562032, 61565013), the Science Foundation of Inner Mongolia, China (Grant No. 2015MS0109), the Inner Mongolia Science Research Fund in Higher Education Institutions, China (NJZZ11166, NJZY12202, NJZY16237), the Production and Research Joint Program of the Baotou Science and Technology Bureau, China (2014X1014-01, 2015Z2011), and the Postgraduate Scientific Research Innovation Program of Inner Mongolia, China (S201710127 (S01)).

References

1. Liu W J 2016 Structural and Physical Properties of Double Perovskite Ln2Ni/CoMnO6 Ph. D. Dissertation (Hefei:University of Science and Technology of China) (in Chinses)[刘文杰 2015双钙钛矿Ln2Ni/CoMnO6体系结构及物性研究 博士学位论文 (合肥:中国科学技术大学)
2. Kang, J.-S., Lee, H.J., Kim, D.H., et al.: Valence and spin states, and the metal-insulator transition in ferromagnetic $La_{2-x}Sr_xMnNiO_6$ (x=0,0.2). Phys. Rev. B. **80**, 045115 (2009)
3. Kim, B., Choi, H.C., Kim, B.H., Min, B.I.: Electronic structure and magnetic properties of hole-carrier-doped La_2MnNiO_6:$La_{2-x}Sr_xMnNiO_6$. Phys. Rev. B. **81**, 224402 (2010)
4. Wang, X.J., Sui, Y., Li, Y., et al.: The influence of the antiferromagnetic boundary on the magnetic property of La $_2NiMnO_6$. Phys. Lett. **95**, 252502 (2009)
5. Zhou, S.M., Guo, Y.Q., Zhao, J.Y., et al.: Appl. Phys. Lett. **96**, 262507 (2010)
6. Zhao, S.Y., Shi, L., Zhou, S.M., et al.: J. Appl. Phys. **106**, 123901 (2009)
7. Guo, Y.Q., Shi, L., Zhou, S.M., et al.: Phys. D: ApplPhys. **46**, 175302 (2013)
8. Wang, W.Q., Xiang, J.Y., Wu, K.H., Wan, S.L., Zhao, J.J., Lu, Y.: J. Rare Earths. **36**(06), 39–44 (2015) (in Chinese)[王文清, 向俊尤, 武柯含, 万素磊, 赵建军, 鲁毅2015 稀土 36(06), 39–44]
9. Asai, K., Fujiyoshi, K., Nishimori, N., et al.: Phys Soc Jpn. **67**, 4218–4228 (1998)
10. Wan, S.L., He, L.M., Xiang, J.Y., Wang, Z.G., Xing, R., Zhang, X.F., Lu, Y., Zhao, J.J.: Acta Phys. Sin. **23**(63), 336–340 (2014) (in Chinese)[万素磊, 何利民, 向俊尤, 王志国, 邢茹, 张雪峰, 鲁毅, 赵建军 2014 物理学报23(63)336-340]
11. Mandal, P.R., Nath, T.K.: MaterResExpress. **2**, 066101 (2015)
12. He, L.M., Ji, Y., Lu, Y., Wu, H.Y., Zhang, X.F., Zhao, J.J.: Acta Phys. Sin. **14**(63), 329–333 (2014) (in Chinese)[何利民, 冀钰, 鲁毅, 吴鸿业, 张雪峰, 赵建军2014 物理学报14(63)329-333]
13. Amit Kumar Singh, Samta Chauhan, Saurabh Kumar Srivastava, etal. Solid State Communication, 2016
14. Sarma, D.D., Ray, S., Tanaka, K., et al.: Phys. Rev. Lett. **98**, 157205 (2007)
15. Sanyal, P., Tarat, S., Majumdar, P., et al.: Eur. Phys. J. B. **65**, 39 (2008)
16. Dass, R.I., Yan, J.-Q., Goodenough, J.B.: Phys.Rev.B. **68**, 0664415 (2003)
17. García-Hernández, M., Martínez, J.L., Martínez-Lope, M.: J. Phys. Rev. Lett. 862443 (2001)
18. Meneghini, C., Ray, S., Liscio, F.: Phys. Rev. Lett. **103**, 046403 (2009)
19. Guo, H.Z., Burgess, J., Ada, E., et al.: Phys. Rev. B. **77**, 174423 (2008)
20. Truong, K.D., Laverdiere, J., Singh, M.P., et al.: Phys. Rev. B. **76**, 132413 (2007)
21. Zhou, S.M., Shi, L., Yang, H.P.: etal. Phys. Lett. **91**, 172505 (2007)
22. Nyrissa, S., Rogado, Li, J., et al.: AdvMater. **17**, 2225–2227 (2005)
23. Meiklejohn, W.H., Bean, C.P.: PhysRev. **102**, 1413 (1957)

24. Sun X D, Xv B, Wu H Y, Cao F Z, Zhao J J, Lu Y 2017 Acta Phys. Sin. (66)15p245–252(in Chinese) [孙晓东,徐宝,吴鸿业,曹风泽,赵建军,鲁毅 2017 物理学报(66)15 245–252]
25. Zemni, S., Bassaoui, M., Dhahri, J., et al.: MaterLett. **63**, 489 (2009)
26. Nirmala, R., Mudryk, Y.: Phys. Rev. B. **76**, 014407 (2007)
27. Wang, D.H., Liu, H.D., Tang, S.L., et al.: Solid State Communication. **121**(4), 199–202 (2002)
28. Shi Q Y, Xv S J, Ju J H, Han Z D, Qian B, Jiang X Y 2015 J. Changshu Instit Technol (Natural Sciences) 29 2 (in Chinese)[倩仪, 许淑娟,居晶华,韩志达,钱 斌,江学范2015常熟理工学院学报(自然科学)第29卷第2期, 2015年3月]
29. Yun, H.Q., Xing, R., Sun, X.D., Sun, Y.B., Lu, Y., Zhao, J.J.: Chin J Low Temp Phys. **02**(39), 11–15 (2017) (in Chinese) [云慧琴,邢茹,孙晓东,孙运斌,鲁毅,赵建军2017低温物理学报02(39)11–15]